Electronic supplementary information (ESI)

Highly Efficient Photothermal Heating *via* Edge-Defects in Boron Quantum Dots

Li Wang,[a,b†] Si-Min Xu,[c†] Shanyue Guan,[a*] Xiaozhong Qu,[b*] Geoffrey I.N. Waterhouse,[d] Shan He[e] and Shuyun Zhou[a]

[a]*Key Laboratory of Photochemical Conversion and Optoelectronic Materials, Technical Institute of Physics and Chemistry, Chinese Academy of Sciences, Beijing, 100190, P. R. China.*

[b]*University of Chinese Academy of Sciences, Beijing 100190, P. R. China.*

[c]*State Key Laboratory of Chemical Resource Engineering, Beijing University of Chemical Technology, Beijing 100029, P. R. China.*

[d]*School of Chemical Sciences, The University of Auckland, Auckland 1142, New Zealand.*

[e]*Beijing Technology and Business University, Beijing, 100148, P. R. China.*

[†]*These authors equally contributed to this work.*

E-mail: guanshanyue@mail.ipc.ac.cn; quxz@iccas.ac.cn.

Experimental Section

Reagents and Chemicals

Boron powder (>95%), Calcein-AM (Cal-AM) and propidium iodide (PI) were purchased from Sigma-Aldrich Corporation. Dulbecco's modified eagle's medium (DMEM), fetal bovin serum (FBS) and phosphate buffer solution (PBS) were obtained from Beijing Solarbio Science and Technology Co., Ltd. A Cell Counting Kit (CCK-8) was purchased from Dojindo China Co., Ltd. Deionized (DI) water was used in all experiments.

Synthesis of B QDs

The commercial boron powder was dispersed in DI water at concentration of 1 mg/mL. The dispersion was then sonicated for 10 h in an ice-bath, after which the dispersion was centrifuged at 10,000 rpm for 20 min. The bulk boron that collected in the bottom of the centrifuge was discarded, whilst the supernatant containing the B QDs was collected and stored for subsequent use.

In vitro experiments

The in vitro cytotoxicity of the B QDs were assessed applied different cell lines (Hela, MCF-7 and HepG-2). Cells were first incubated in a 25 cm^2 cell-culture flask and then subsequently seeded into a 96-well plate (1×10^4 cells/well) by pipetting. After seeding the 96-well plate, we exposed the Hela, MCF-7 or HepG-2 cells to series doses of B QDs (or the other reference materials) for 24 h. After further incubation for 24 h, a mixture of CCK-8 and DMEM (1:10) was added to each well. The cell viability was then calculated as the ratio of the absorbance of the wells versus the absorbance of the control. Absorbances at 450 nm were measured using a Biotek synergy H1 (USA). The cytotoxicity was calculated by averaging six individual reads in six identical wells.

In vivo experiments

All animal procedures complied with institutional animal regulations. All animal procedures were conducted according to institutional regulations regarding animal use and care, as approved by the Model Animal Research Center of Institute of Process Engineering, Chinese Academy of Sciences. Male nude Balb/c mice were purchased from Beijing HFK Bioscience Co., Ltd. 2×10^6 Hela cells suspended in 200 μL DMEM were injected subcutaneously in the right lateral back of each mouse. The mice bearing Hela tumors were treated when the tumor volume reached ~100 mm^3. The mice were randomized into 3 groups (n = 5) and were dosed at 10 mg/kg *via* intravenous injection. The groups were (1) PBS, (2) B QDs, and (3) B QDs+NIR. Three hours later, the tumor sites of mice in the B QDs+NIR group were irradiated with NIR (808 nm, 1 W) for 10 min. Subsequently, the tumor size and the body weight of the animals in the three groups were monitored every 2 days for 20 days. No further NIR treatments were performed. The volume of the tumor was calculated by the equation of $V=\frac{L\cdot W^2}{2}$ where L is the length and W is the width of the tumor measured using a caliper. Twenty days after therapy, the main organs and tumors were harvested from the three groups of mice, with the organs and tumors being dissected and fixed in a 4% formaldehyde solution for 24 h at room temperature. Organ slices were stained with H&E (hematoxylin and eosin) and TUNEL and investigated for histological variations.

Sample characterization

The structures and morphologies of the samples were examined using transmission electron microscopy (TEM, JEOL JEM-2100F operated at 150 kV). Powder X-ray diffraction (XRD) patterns were collected on a Bruker X-ray diffractometer (D8 focus, Cu Kα, λ=0.15178 nm) with the step of 0.1 ° s^{-1}. Fourier transform infrared spectra (FT-IR) were obtained on a Varian Excalibur 3100 FTIR spectrophotometer. XPS was carried out with ESCALAB 250Xi (Thermo Scientific), using an Al Kα X-ray source. Raman spectra were measured on inVia-Reflex (Renishaw). The spectra were excited

using a 532 nm laser. UV-vis absorption spectra were acquired on a Hitachi U-3010 spectrophotometer. Confocal fluorescence images were obtained on a Nikon A1R Eclipse Ti confocal laser scanning microscope with a 40× water immersible objective. A Thermo Multiskan FC was used to investigate cell viability. Photoacoustic imaging was performed on a multispectral optoacoustic tomographic (MSOT) real time imaging system (inVision 128, Germany). A thermal infrared camera (FLIR P620, FLIR Systems Inc, USA) was used to record the infrared thermal images.

Statistical Analysis

Statistical significance was assessed using a one-way ANOVA analysis on SPSS 16.0 software. The difference was considered to be statistically significant if the probability value was less than 0.05 ($p < 0.05$). Mean value and standard deviation (SD) were calculated for triplicate experiments. And data are presented as mean ± SD.

Photothermal Conversion Efficiency Measurements

A quartz cuvette filled with a 1.0 mL dispersion of a sample was irradiated with a 808 nm laser (laser power 1 W, the power density 2 W cm^{-2}, Changchun New Industries Optoelectronics Tech. Co., Ltd, MDL-III-808nm-2W-16090665). The temperature of the dispersion was monitored by a digital thermometer using a thermocouple probe immersed in the dispersion (temperature accuracy ± 0.1 ºC).

The photothermal conversion efficiency (η) was calculated according to a literature method[1]:

$$\eta = \frac{hA(T_{MAX} - T_{surr}) - Q_{dis}}{I(1-10^{-A\lambda})} \quad (2)$$

where T_{MAX} and T_{surr} are the final and ambient temperatures (in ^{o}C) of the dispersion under irradiation, h is the heat transfer coefficient (J cm^{-2}), A represents the surface area (in cm^2) of the cuvette, Q_{dis} is the heat dissipation of solvent (for water, Q_{dis} = 0.056), I is the irradiation laser power (1 W in this case1), and $A\lambda$ is the absorbance at 808 nm. For the calculation of hA, the following equation was used:

$$hA = \frac{\sum c_i m_i}{\tau_S} \tag{3}$$

where c and m represent the mass (1 g) and heat capacity (4.2 J g^{-1}) of water, respectively. The sample system time constant (τ_S) was calculated using the equation:

$$\tau_S = -\frac{t}{\ln\theta} \tag{4}$$

where t is time (in s) and θ is the dimensionless driving force.

Supplementary Figures

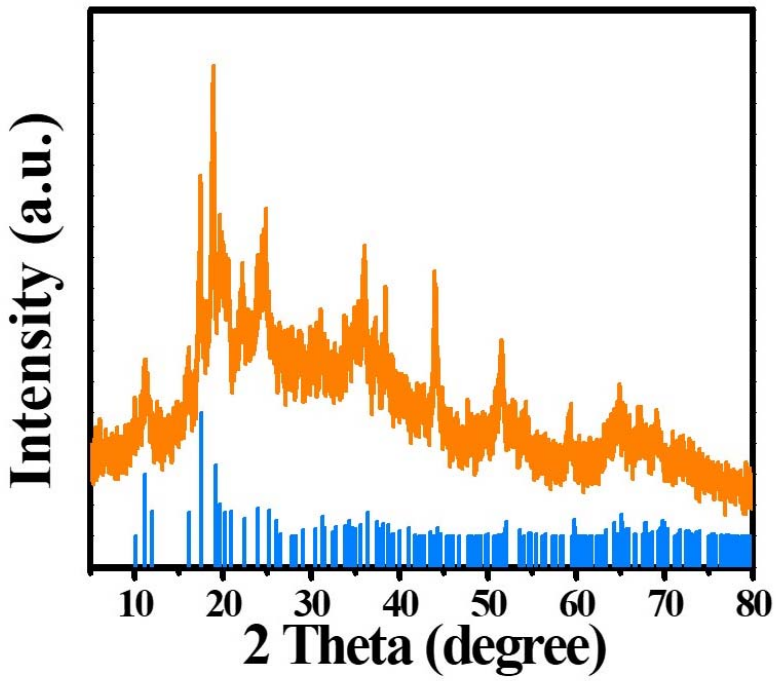

Figure S1. XRD pattern of B QDs and the standard PDF card for B (JCPDS No. 80-0323).

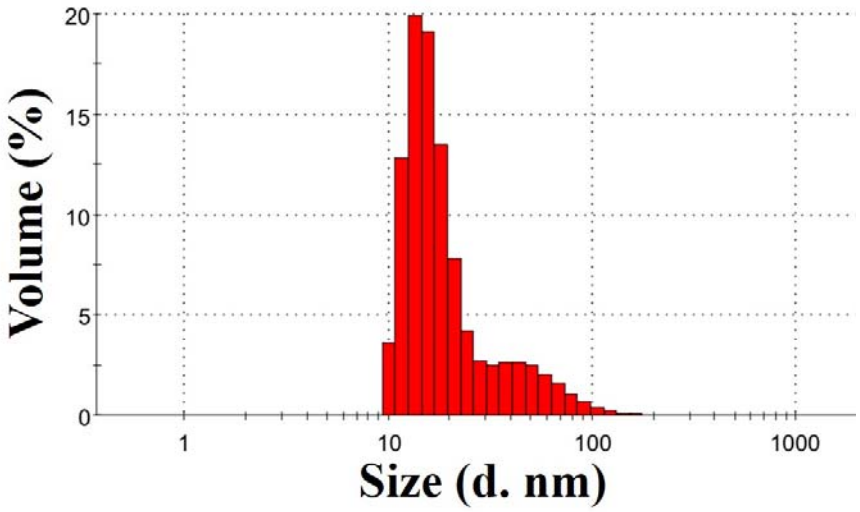

Figure S2. Particle size distribution of B QDs determined by dynamic light scattering (DLS).

Figure S3. The Zeta potential of B QDs in buffered saline solutions at pH=7.

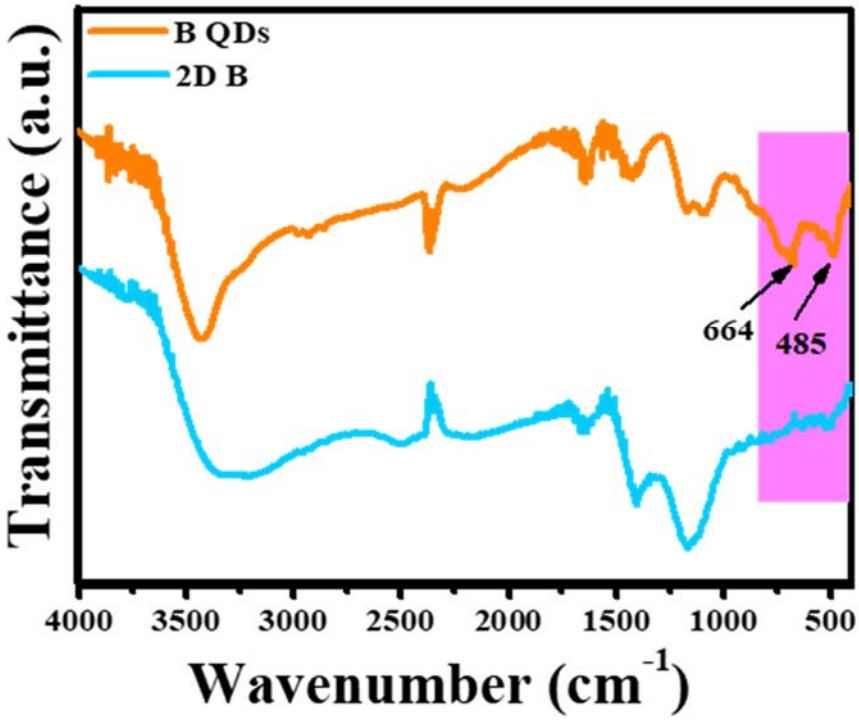

Figure S4. FT-IR spectra for B QDs and 2D B. The spectra have been offset vertically for clarity.

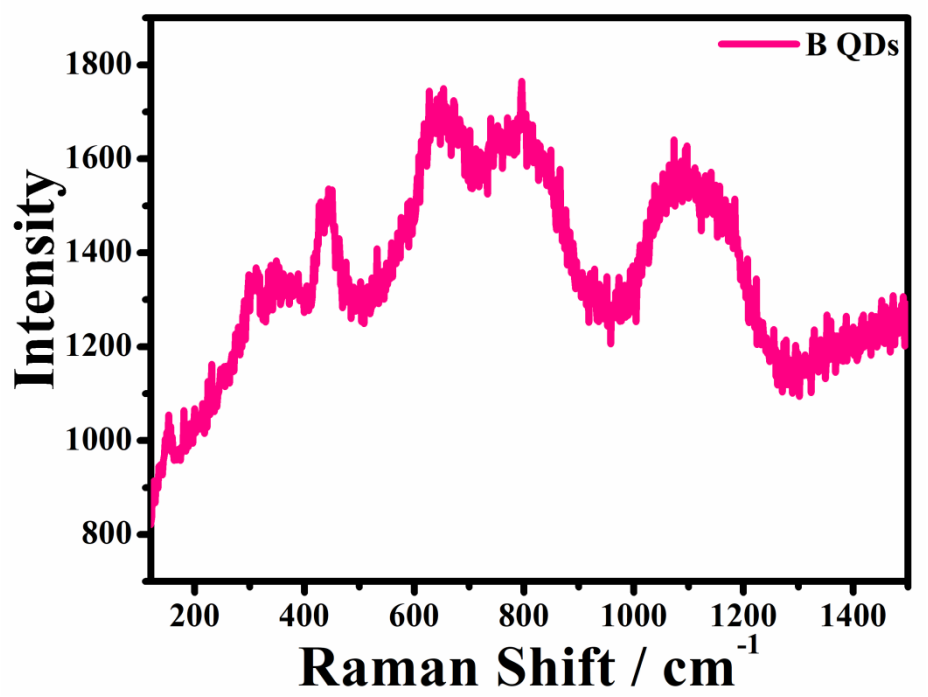

Figure S5. Raman spectrum of B QDs.

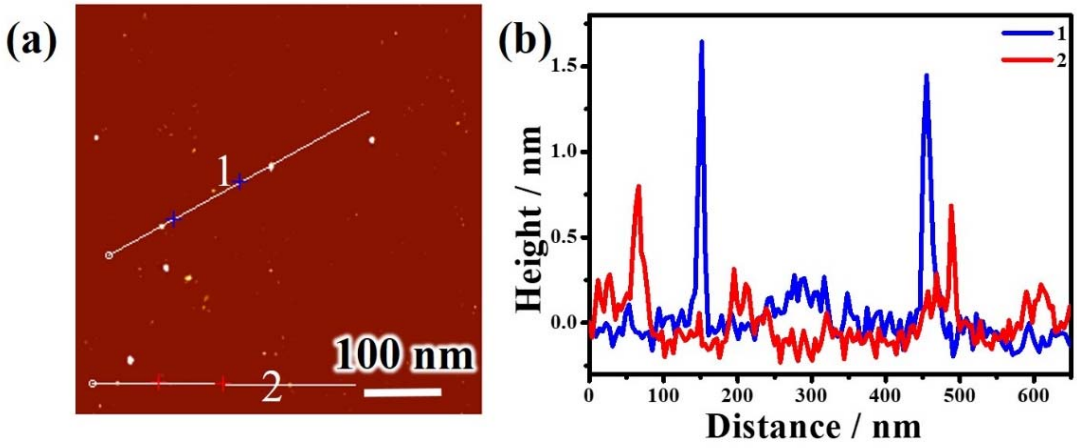

Figure S6. (a) AFM image of B QDs. (b) The corresponding height profiles for B QDs measured along line 1 and line 2 in (a).

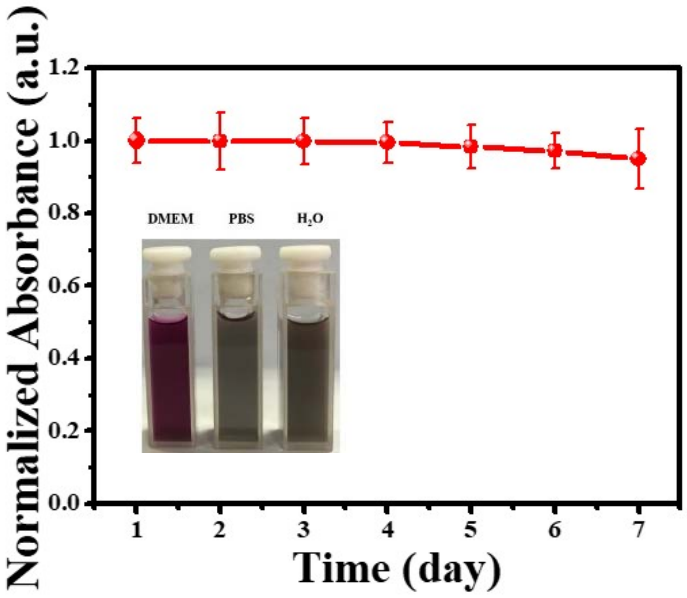

Figure S7. UV-vis absorbance at 808 nm of B QDs in phosphate buffer saline (PBS) over 7 days. (Inset: Digital photograph showing B QDs dispersed in water, PBS and cell culture medium (DMEM).

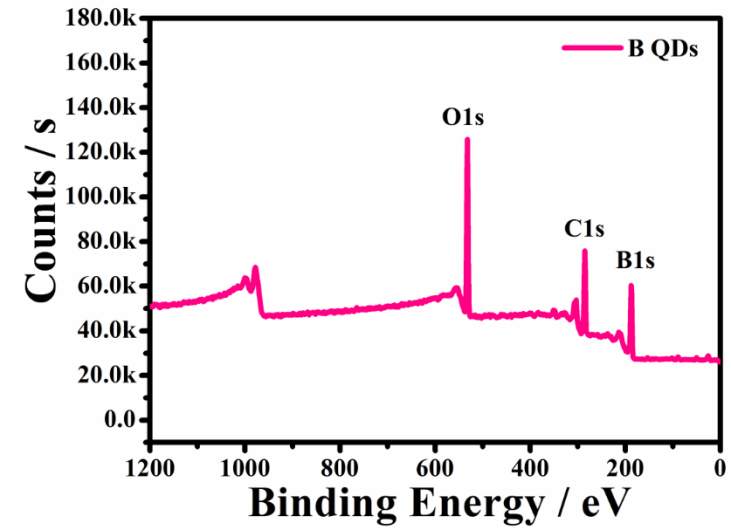

Figure S8. XPS survey spectrum for B QDs.

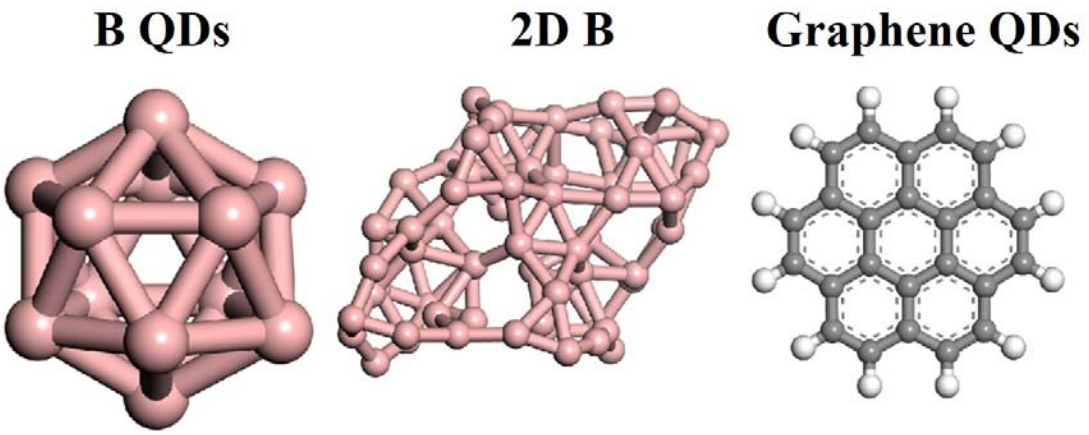

Figure S9. Optimized geometries for the B QDs, 2D B, and Graphene QDs models.

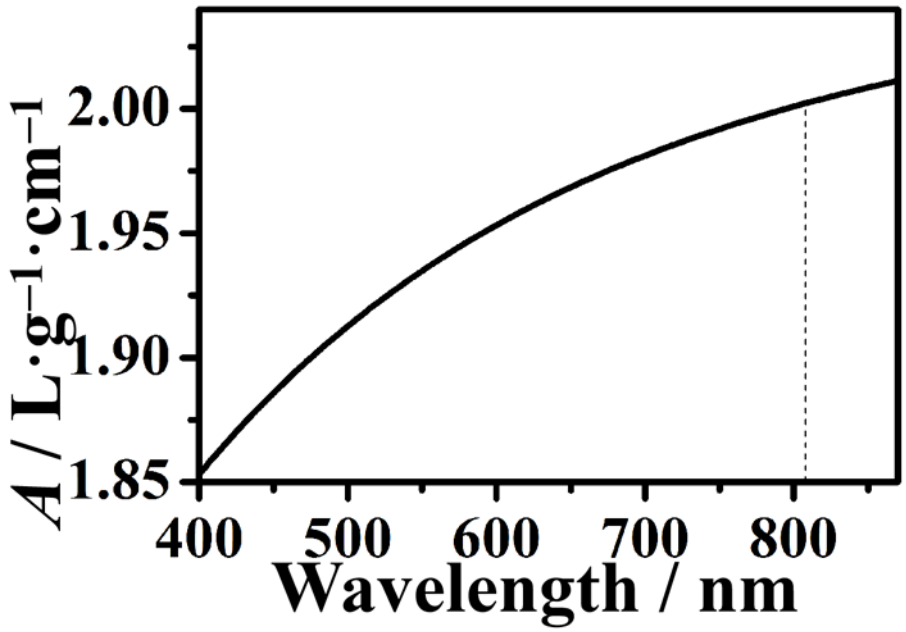

Figure S10. Absorbance of B QDs as a function of the incident wavelength. The NIR wavelength of 808 nm used in PTT is indicated by the dashed line.

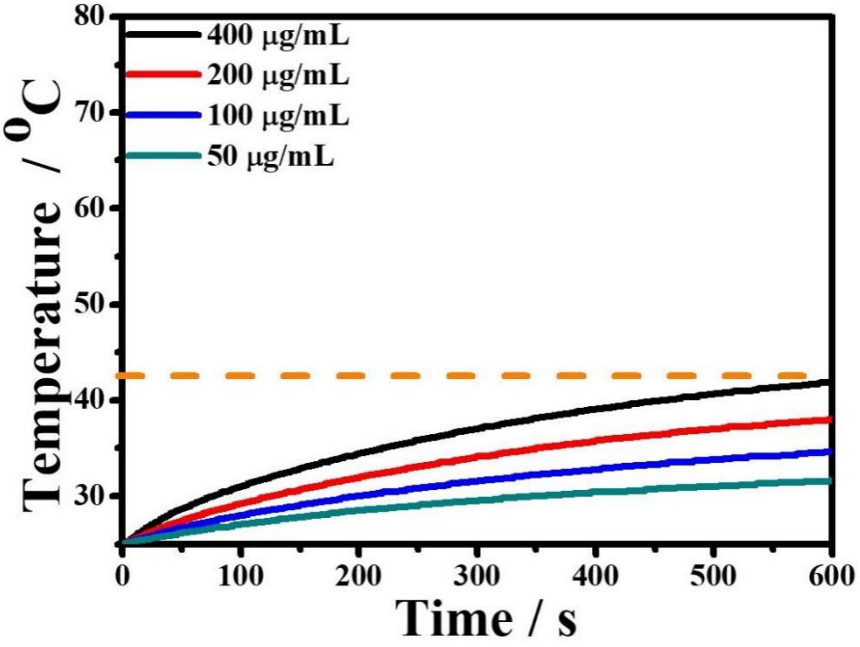

Figure S11. Photothermal heating curves for dispersions of B QDs at various concentrations (50, 100, 200 and 400 μg/mL) under 808 nm laser irradiation (0.5 W).

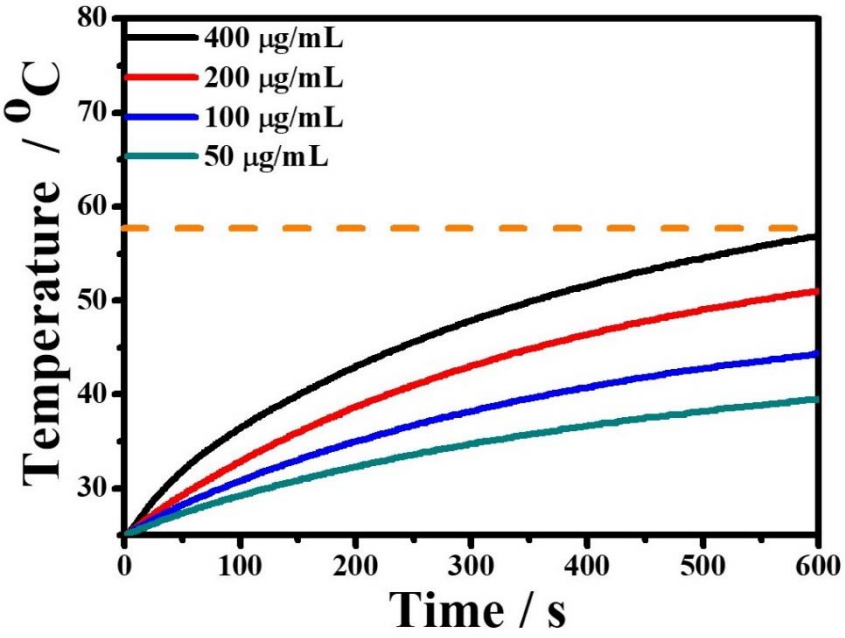

Figure S12. Photothermal heating curves of B QDs at various concentrations (50, 100, 200 and 400 μg/mL) under 808 nm laser irradiation (0.8 W).

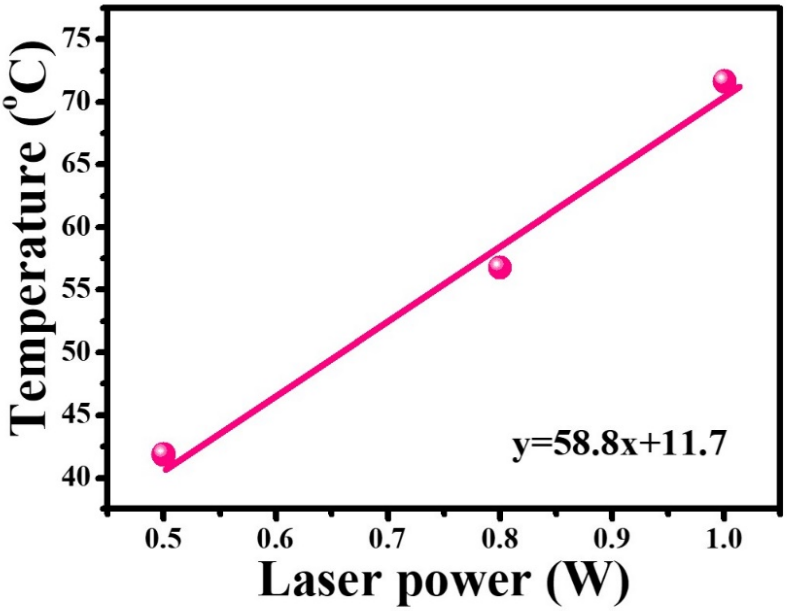

Figure S13. Plot showing the temperature of a B QDs dispersion (400 μg/mL) after laser irradiation for 10 min at different laser powers.

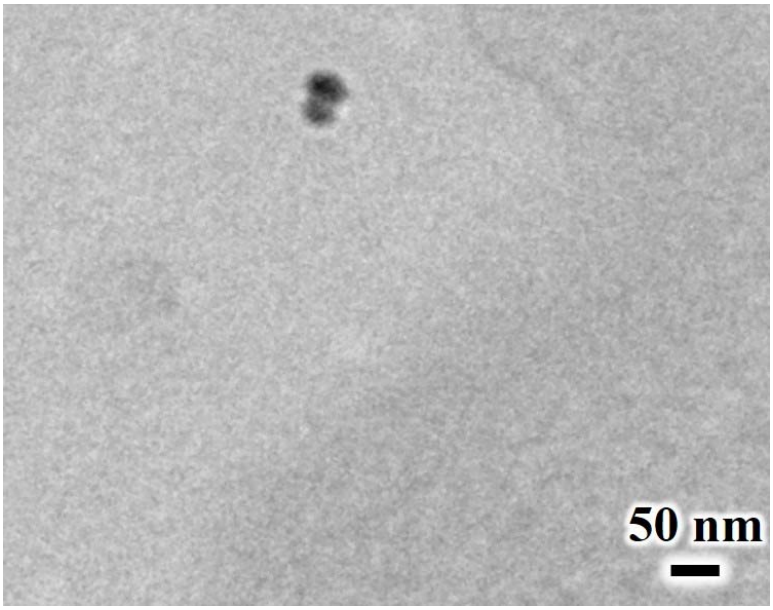

Figure S14. The TEM image of the cell after incubation with B QDs.

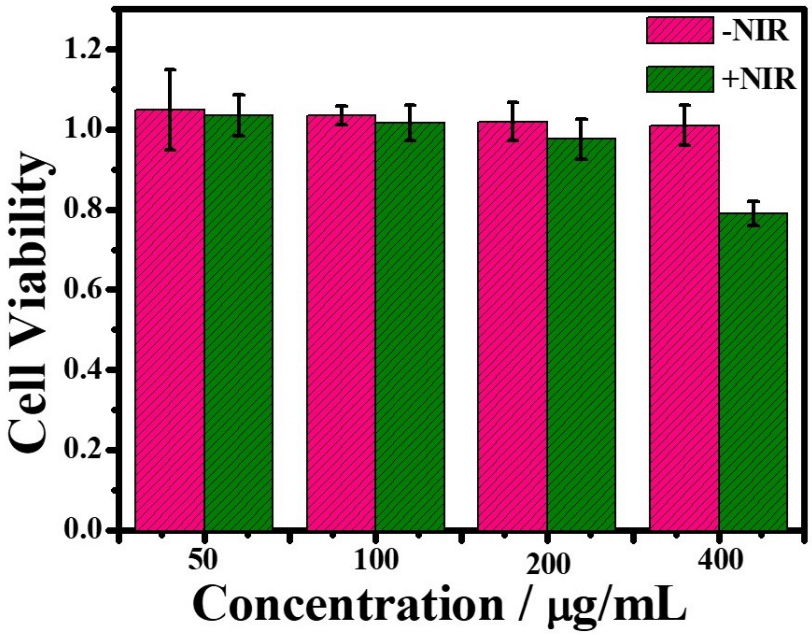

Figure S15. The viability of Hela cells incubated with B QDs (concentration 50, 100, 200 and 400 μg/mL). The NIR treatment was 808 nm (0.5 W) for 10 min.

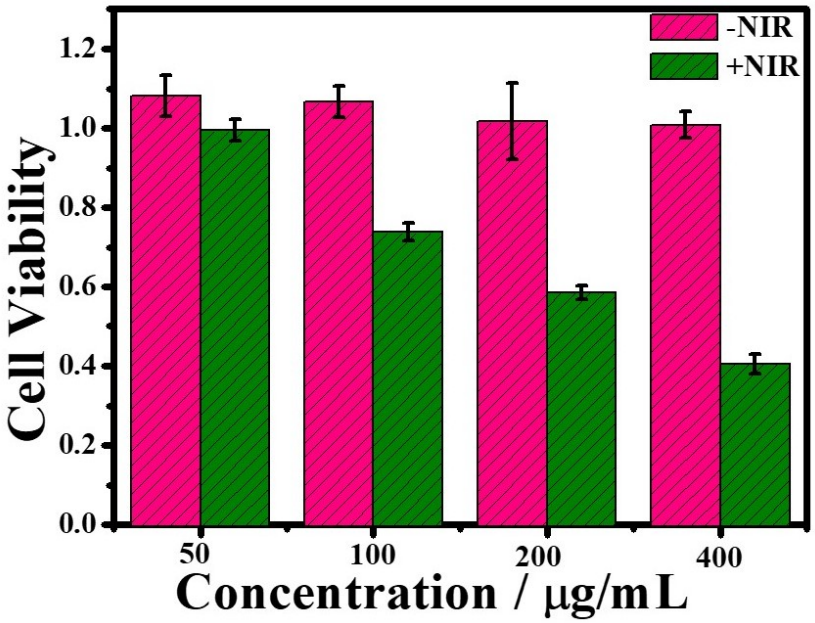

Figure S16. The viability of Hela cells incubated with B QDs (concentrations 50, 100, 200 and 400 μg/mL). The NIR treatment was 808 nm (0.8 W) for 10 min.

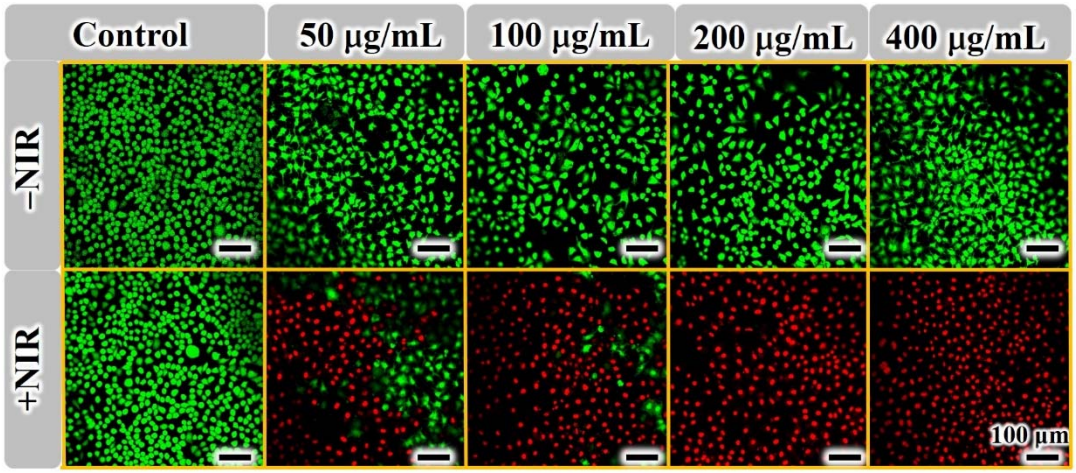

Figure S17. Confocal images of control, B QDs, B QDs+NIR (B QDs concentrations were 50, 100, 200 and 400 μg/mL. Live and dead Hela cells are shown in green and red (Calcein AM/PI), respectively.

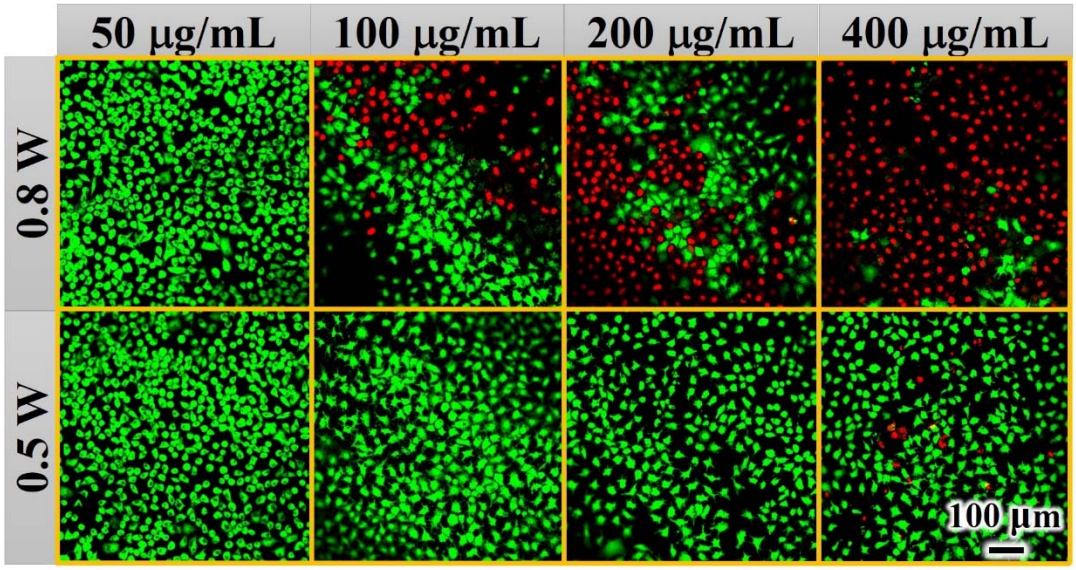

Figure S18. Confocal imaging of Hela cells treated with B QDs+NIR (B QDs concentrations 50, 100, 200 and 400 μg/mL, and 808 nm NIR (0.5 W or 0.8 W). Live and dead Hela cells appear green and red (Calcein AM/PI), respectively.

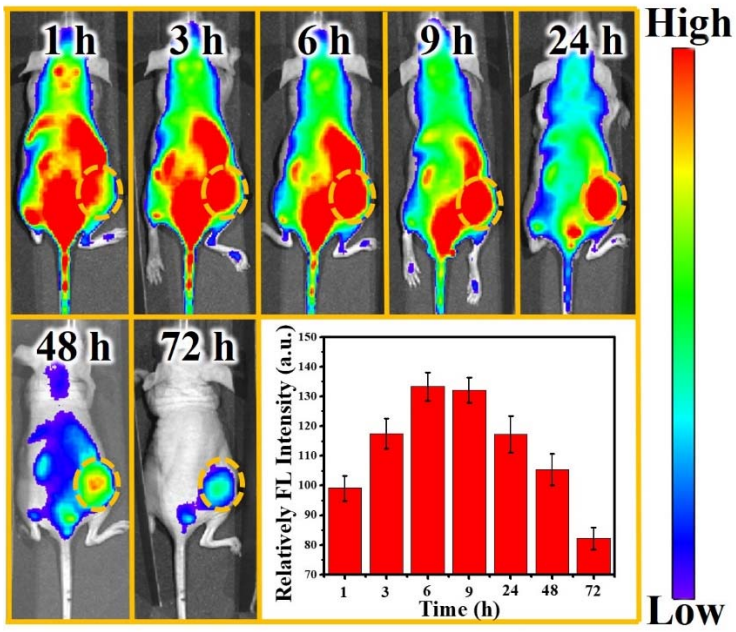

Figure S19. *In vivo* FL images of Hela tumor-bearing mice taken after *i.v.* injection of the B QDs/ICG.

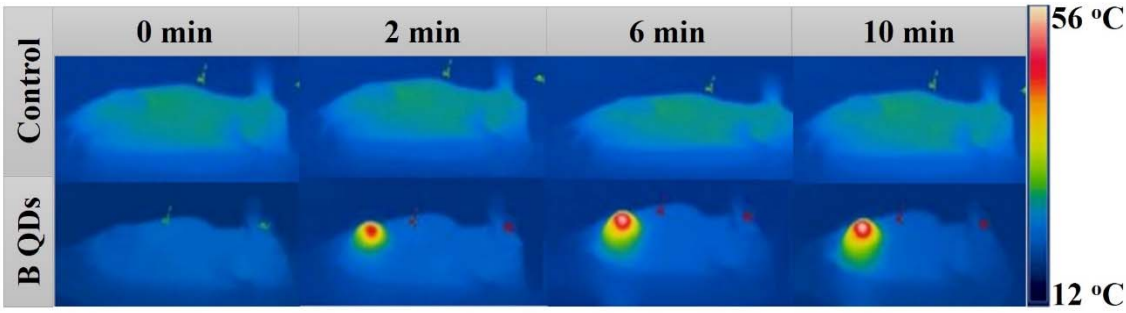

Figure S20. NIR thermal images of Hela tumor-bearing mice *i.v.* injected with B QDs and PBS under NIR irradiation (808 nm).

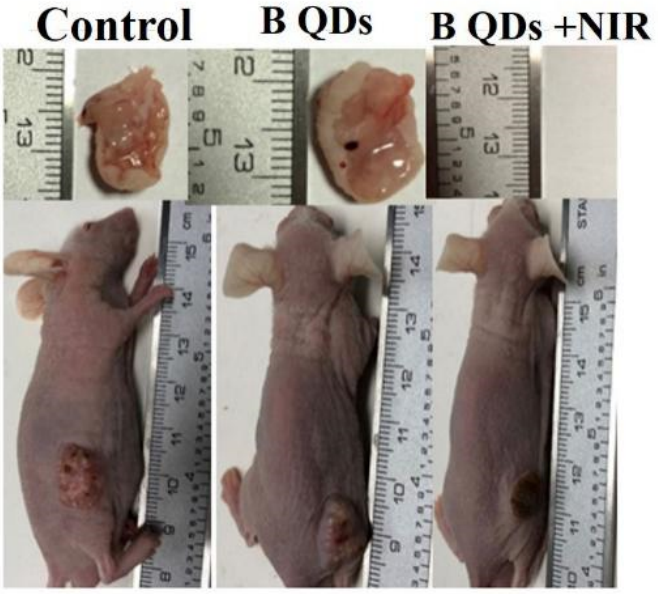

Figure S21. Representative images of tumor-bearing mice and their excised tumors 20 days after various treatments.

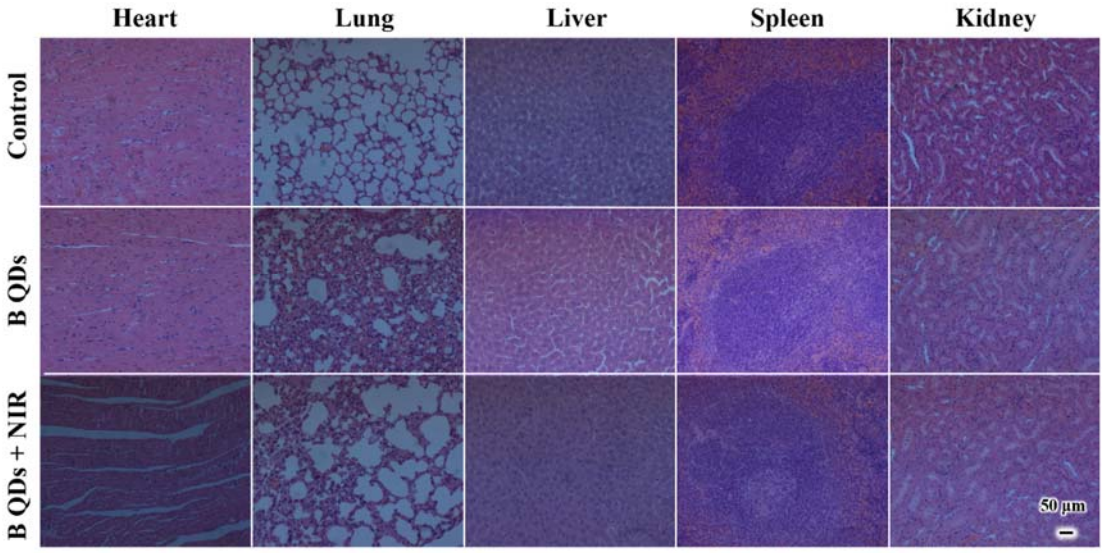

Figure S22. H&E-stained images of the main organ tissues from mice in the different treatment groups.

Supplementary Table

Table S1. Descartes coordinates of the optimized geometries for B QDs.

element	Descartes coordinates / Å		
	ξ	ψ	ζ
B	–0.7405	–0.8396	–1.1542
	–0.7404	1.3639	0.4469
	–0.7422	0.8413	–1.1510
	–1.7634	0.0002	0.0040
	0.7337	0.0020	–1.4225
	0.7390	–1.3660	–0.4458
	0.7377	1.3679	–0.4432
	0.7438	0.8384	1.1520
	0.7421	–0.8424	1.1510
	1.7640	0.0002	–0.0056
	–0.7417	–1.3643	0.4428
	–0.7320	–0.0015	1.4256
	–0.7404	–0.8396	–1.1542

Table S2. Descartes coordinates of the optimized geometries for 2D B.

element	Descartes coordinates / Å			Descartes coordinates / Å		
	x	*y*	*z*	*x*	*y*	*z*
B	–3.1197	2.5095	2.1476	–6.7695	–0.0110	2.0849
	1.8765	2.4830	0.4274	–2.2663	–0.0045	0.0576
	2.8518	2.5199	–1.0917	–1.3646	–0.0048	–1.5543
	–1.8718	3.2877	2.5425	–5.5601	0.9647	2.0389
	0.3767	1.5568	0.3123	–3.7500	–0.9315	–0.0944
	0.2459	0.9129	–1.3756	–3.8755	–1.4582	–1.8095
	–1.5746	1.6435	2.3287	–5.5550	–0.9798	2.0425
	0.2293	3.3294	0.2559	–3.7564	0.9134	–0.1000
	0.2899	3.8021	–1.3793	–3.8861	1.4289	–1.8176
	2.5892	2.2900	1.9064	–1.6201	–0.0003	1.5938
	0.2469	2.3852	–2.3790	–3.8609	–0.0167	–2.7342
	–0.7090	2.3514	–0.8875	–4.7810	–0.0161	–1.2762
	–0.7035	3.6473	1.5861	–4.2890	1.6814	1.3466
	1.6411	1.6411	–2.1923	–2.4652	–0.8295	–2.6540
	–2.3066	3.3063	–1.1417	–6.3718	0.8339	–1.5098
	–0.1633	0.8470	1.7335	–4.2812	–1.6911	1.3566
	1.6676	3.2974	–2.1218	–2.4710	0.8064	–2.6586
	–2.2893	1.4373	–1.0401	–6.3634	–0.8760	–1.5063
	1.1721	0.0054	2.6218	–3.1063	–2.5056	2.1637
	6.1407	0.0127	0.8628	1.8944	–2.4612	0.4430
	6.6779	–0.0047	–0.6571	2.8744	–2.4961	–1.0741
	2.6220	0.8359	2.8284	–1.5709	–1.6566	2.3210
	4.5581	–0.8645	0.7603	0.2571	–3.3174	0.2718
	4.3208	–1.6040	–1.0046	0.3211	–3.7975	–1.3632
	2.6137	–0.8119	2.8548	–1.8241	–3.2398	2.5576
	4.5524	0.8784	0.7395	0.3883	–1.5494	0.3202
	4.3064	1.5686	–1.0503	0.2581	–0.9110	–1.3714
	6.5852	0.0362	2.4803	2.5882	–2.2528	1.9287
	4.3435	–0.0307	–1.9079	0.2706	–2.3865	–2.3686
	3.4602	–0.0135	–0.4158	–0.6894	–2.3532	–0.8769
	3.9726	1.5046	2.0851	–0.1588	–0.8435	1.7359
	5.7033	–0.8645	–1.7229	1.6980	–3.2874	–2.1050
	1.8290	0.9978	–0.5685	–2.2786	–1.4505	–1.0321
	3.9736	–1.4555	2.1090	–0.6548	–3.6254	1.6094
	5.6943	0.8204	–1.7458	1.6603	–1.6317	–2.1820
	1.8399	–0.9821	–0.5603	–2.2833	–3.3195	–1.1241

Table S3. Descartes coordinates of the optimized geometries for Graphene QD.

element	Descartes coordinates / Å			element	Descartes coordinates / Å		
	x	*y*	*z*		*x*	*y*	*z*
C	–3.7438	–0.0561	–0.0001	H	–4.7620	–0.4342	–0.0001
	–3.5133	1.2944	–0.0001		–4.3487	1.9885	–0.0001
	–2.1899	1.8170	–0.0001		–2.7570	3.9067	–0.0001
	–1.9205	3.2140	–0.0001		–0.4520	4.7602	–0.0001
	–0.6356	3.6896	–0.0001		–3.8967	–2.7713	–0.0001
	–2.8777	–2.3952	0.0000		–2.0050	–4.3409	0.0000
	–2.6686	–0.9879	–0.0001		2.0050	4.3409	0.0000
	–1.3375	–0.4951	0.0000		3.8967	2.7713	0.0001
	–1.8233	–3.2700	0.0000		0.4520	–4.7602	0.0001
	–0.4787	–2.8048	0.0000		2.7570	–3.9067	0.0001
	–1.0976	0.9106	0.0000				
	0.2399	1.4058	0.0000				
	0.4787	2.8048	0.0000				
	1.8233	3.2700	0.0000				
	–0.2399	–1.4058	0.0000				
	1.0976	–0.9106	0.0000				
	1.3375	0.4951	0.0000				
	2.6686	0.9879	0.0001				
	2.8777	2.3952	0.0001				
	0.6356	–3.6896	0.0001				
	1.9205	–3.2140	0.0001				
	2.1899	–1.8170	0.0001				
	3.5133	–1.2944	0.0001				
	3.7438	0.0561	0.0001				

Table S4. The photothermal conversion efficiency of various PTT agents.

Agents	Wavelength	η	ref
Antimonene QDs	808 nm	45.5%	[2]
Carbon Dots	671 nm	38.5%	[3]
MOF-Polydopamine	808 nm	41.3%	[4]
free ICG	808 nm	15%	[5]
Ti_3C_2 nanosheets	808 nm	30.6%	[6]
Au NRs	808 nm	21%	[7]
B nanosheets	808 nm	42.5%	[8]
carbon nanospheres	808 nm	35.7%	[9]
polypyrrole nanosheets	1064 nm	64.6%	[10]
CuS@MSN NPs	980 nm	28.8%	[11]
$WO_{2.9}$ Nanorods	808 nm	44.9%	[12]
Fe@γ-Fe_2O_3@H-TiO_2	808 nm	20.8%	[13]
Cu_7S_4–Au	808 nm	64.4%	[14]
MOF Nanoshuttle	635 nm	33.7%	[15]
semiconducting polymer nanococktail	808 nm	35%	[16]
semiconducting polymer nanoenzyme	808 nm	42.8%	[17]
UCNP@NGO	980 nm	40%	[18]
Polydopamine Mn^{2+} nanoparticles	808 nm	46%	[19]
Polymer Dots	660 nm	45%	[20]
Ge QDs	808 nm	45.9%	[21]
B QDs	**808 nm**	**57%**	**This work**

References

1. Q. Tian, F. Jiang, R. Zou, Q. Liu, Z. Chen, M. Zhu, S. Yang, J. Wang, J. Wang and J. Hu, *ACS Nano*, 2011, **5**, 9761–9771.

2. W. Tao, X. Ji, X. Xu, M. A. Islam, Z. Li, S. Chen, P. E. Saw, H. Zhang, Z. Bharwani, Z. Guo, J. Shi and O. C. Farokhzad, *Angew. Chem. Int. Ed.*, 2017, **56**, 11896–11900.

3. J. Ge, Q. Jia, W. Liu, L. Guo, Q. Liu, M. Lan, H. Zhang, X. Meng and P. Wang, *Adv. Mater.*, 2015, **27**, 4169–4177.

4. D. Wang, H. Wu, J. Zhou, P. Xu, C. Wang, R. Shi, H. Wang, H. Wang, Z. Guo and Q. Chen, *Adv. Sci.*, 2018, 1800287.

5. M. Zheng, P. Zhao, Z. Luo, P. Gong, C. Zheng, P. Zhang, C. Yue, D. Gao, Y. Ma and L. Cai, *ACS Appl. Mater. Interfaces*, 2014, **6**, 6709–6716.

6. H. Lin, X. Wang, L. Yu, Y. Chen and J. Shi, *Nano Lett.*, 2017, **17**, 384–391.

7. J. Zeng, D. Goldfeld and Y. Xia, *Angew. Chem. Int. Ed.*, 2013, **52**, 4169–4173.

8. X. Ji, N. Kong, J. Wang, W. Li, Y. Xiao, S. T. Gan, Y. Zhang, Y. Li, X. Song, Q. Xiong, S. Shi, Z. Li, W. Tao, H. Zhang, L. Mei and J. Shi, *Adv. Mater.*, 2018, 1803031.

9. Y. Weng, S. Guan, L. Wang, X. Qu and S. Zhou, *J. Mater. Chem. B*, 2019, **7**, 1920.

10. X. Wang, Y. Ma, X. Sheng, Y. Wang and H. Xu, *Nano Lett.*, 2018, **18**, 2217.

11. N. Li, Q. Sun, Z. Yu, X. Gao, W. Pan, X. Wan and B. Tang, *ACS Nano*, 2018, **12**, 5197.

12. L. Sun, Z. Li, R. Su, Y. Wang, Z. Li, B. Du, Y. Sun, P. Guan, F. Besenbacher and M. Yu, *Angew. Chem. Int. Ed.* 2018, **57**, 10666−10671.

13. M. Wang, K. Deng, W. Lu, X. Deng, K. Li, Y. Shi, B. Ding, Z. Cheng, B. Xing, G. Han, Z. Hou and J. Lin, *Adv. Mater.*, 2018, **30**, 1706747.

14. J. Cui, R. Jiang, C. Guo, X. Bai, S. Xu and L. Wang, *J. Am. Chem. Soc.*, 2018, **140**, 5890–5894.

15. K. Zhang, X. Meng, Y. Cao, Z. Yang, H. Dong, Y. Zhang, H. Lu, Z. Shi and X. Zhang, *Adv. Funct. Mater.*, 2018, **28**, 1804634.

16. X. Zhen, C. Xie and K. Pu, *Angew. Chem. Int. Ed.*, 2018, **57**, 3938–3942.

17. J. Li, C. Xie, J. Huang, Y. Jiang, Q. Miao and K. Pu, *Angew. Chem. Int. Ed.*, 2018, **57**, 3995–3998.

18. P. Li, Y. Yan, B. Chen, P. Zhang, S. Wang, J. Zhou, H. Fan, Y. Wang and X. Huang, *Biomater. Sci.*, 2018, **6**, 877–884.

19. J. Feng, Z. Xu, F. Liu, Y. Zhao, W. Yu, M. Pan, F. Wang and X. Liu, *ACS Nano*, 2018, **12**, 12888.

20. K. Chang, Y. Liu, D. Hu, Q. Qi, D. Gao, Y. Wang, D. Li, X. Zhang, H. Zheng, Z. Sheng and Z. Yuan, *ACS Appl. Mater. Interfaces*, 2018, **10**, 7012–7021.

21. J. Ouyang, C. Feng, X. Ji, L. Li, H. K. Gutti, N. Y. Kim, D. Artzi, A. Xie, N. Kong, Y. N. Liu, G. J. Tearney, X. Sui, W. Tao and O. C. Farokhzad, *Angew. Chem. Int. Ed.*, 2019, **58**, 1–7.